

# RNF17 blocks promiscuous activity of PIWI proteins in mouse testes

Kaja A. Wasik,<sup>1,2</sup> Oliver H. Tam,<sup>1</sup> Simon R. Knott,<sup>1,2</sup> Ilaria Falciatori,<sup>1,2</sup> Molly Hammell,<sup>1</sup> Vasily V. Vagin,<sup>1,2</sup> and Gregory J. Hannon<sup>1,2,3</sup>

<sup>1</sup>Watson School of Biological Sciences, <sup>2</sup>Howard Hughes Medical Institute, Cold Spring Harbor Laboratory, New York 11724, USA;

<sup>3</sup>Cancer Research UK Cambridge Institute, Li Ka Shing Centre, University of Cambridge, Cambridge CB2 0RE, United Kingdom

**PIWI proteins and their associated piRNAs protect germ cells from the activity of mobile genetic elements. Two classes of piRNAs—primary and secondary—are defined by their mechanisms of biogenesis. Primary piRNAs are processed directly from transcripts of piRNA cluster loci, whereas secondary piRNAs are generated in an adaptive amplification loop, termed the ping-pong cycle. In mammals, piRNA populations are dynamic, shifting as male germ cells develop. Embryonic piRNAs consist of both primary and secondary species and are mainly directed toward transposons. In meiotic cells, the piRNA population is transposon-poor and largely restricted to primary piRNAs derived from pachytene piRNA clusters. The transition from the embryonic to the adult piRNA pathway is not well understood. Here we show that RNF17 shapes adult meiotic piRNA content by suppressing the production of secondary piRNAs. In the absence of RNF17, ping-pong occurs inappropriately in meiotic cells. Ping-pong initiates piRNA responses against not only transposons but also protein-coding genes and long noncoding RNAs, including genes essential for germ cell development. Thus, the sterility of *Rnf17* mutants may be a manifestation of a small RNA-based autoimmune reaction.**

[*Keywords:* piRNAs; PIWI proteins; transposons; spermatogenesis; germ cells]

Supplemental material is available for this article.

Received May 6, 2015; revised version accepted June 3, 2015.

The piRNA pathway comprises an elegant, small RNA-based innate immune system, generally tasked with protecting germ cell genomes against the activity of mobile genetic elements (Malone and Hannon 2009; Siomi et al. 2011). The specificity of the pathway derives from piRNA clusters, which direct the selective silencing of parasitic DNA elements (Aravin et al. 2007). The piRNA pathway and its protective role are deeply conserved in animals; impairment most often results in the derepression of normally silent transposons and loss of functional germ cells (Klattenhoff and Theurkauf 2008; Pillai and Chuma 2012).

piRNAs function through their association with PIWI proteins. In mice, three PIWI proteins—MILI, MIWI, and MIWI2—are expressed in developing male germ cells, and all are essential for proper germ cell development (Kuramochi-Miyagawa et al. 2004; Carmell et al. 2007; Pillai and Chuma 2012). During embryogenesis, germ cells undergo an epigenetic reprogramming that requires the erasure and re-establishment of DNA methylation patterns genome-wide (Aravin et al. 2008; Kota and Feil 2010; Bao and Yan 2012). A key element of reprogramming is the recognition of transposons and the deposition

of heritable DNA methylation marks that maintain mobile elements in a silent state (Aravin et al. 2008; Castaneda et al. 2011; Bao and Yan 2012). This requires the piRNA pathway; specifically, two embryonically expressed PIWI family proteins: MILI and MIWI2 (Aravin et al. 2008; Bao and Yan 2012). In embryonic germ cells, MILI and MIWI2 are primed by primary piRNAs derived from a variety of dispersed transposon-rich loci (Aravin et al. 2008). Once primed, these proteins engage in the adaptive ping-pong cycle, which produces secondary piRNAs (Aravin et al. 2007; Siomi et al. 2011), perhaps honing the pathway against active element subfamilies (Aravin et al. 2008).

Shortly after mice are born, male germ cells initiate meiosis (Chuma and Nakano 2013), and piRNA populations shift from a collection of primary and secondary species, enriched for transposon content, to mainly primary piRNAs, which are derived from a collection of discrete genomic loci, termed pachytene piRNA clusters (Aravin et al. 2006; Girard et al. 2006; Lau et al. 2006). These mainly produce uniquely mapping piRNAs that match only the

**Corresponding authors:** [greg.hannon@cruk.cam.ac.uk](mailto:greg.hannon@cruk.cam.ac.uk), [vagin@cshl.edu](mailto:vagin@cshl.edu)  
Article published online ahead of print. Article and publication date are online at <http://www.genesdev.org/cgi/doi/10.1101/gad.265215.115>.

© 2015 Wasik et al. This article is distributed exclusively by Cold Spring Harbor Laboratory Press for the first six months after the full-issue publication date (see <http://genesdev.cshlp.org/site/misc/terms.xhtml>). After six months, it is available under a Creative Commons License (Attribution-NonCommercial 4.0 International), as described at <http://creativecommons.org/licenses/by-nc/4.0/>.

loci from which they are derived (Aravin et al. 2006; Girard et al. 2006). PIWI protein expression also shifts, with MIWI2 being lost, and MIWI joining MILI as the major piRNA-binding partner (Fig. 1A; Aravin and Hannon 2008). MIWI is required for successful spermatogenesis (Deng and Lin 2002), implying that meiotic piRNAs have a critical role in germ cell development. However, the precise functions of meiotic piRNAs remain a topic of debate.

PIWI proteins function in conjunction with an array of accessory factors. One such family of proteins, the Tudors, is particularly important, with functions that are well conserved across a range of species (Siomi et al. 2010; Chen et al. 2011). Tudor proteins recognize methylated arginines present on PIWI proteins through their tudor domains and facilitate the localization of PIWI to RNA processing granules. Tudors often have additional domains, opening the possibility that they could perform any of a variety of functions in the formation of PIWI-piRNA complexes (Chen et al. 2011).

Here we assessed the role of a Tudor family member, RNF17, and found that it helps to shape piRNA content throughout adult spermatogenesis. RNF17 associates with pachytene piRNA precursors, facilitates piRNA biogenesis, and represses secondary piRNA amplification in

adult gonads. Deletion of RNF17 unleashes ping-pong during meiosis and enriches meiotic piRNA populations with transposon-derived secondary piRNAs. piRNAs that arise specifically in mutant animals also derive from a wide range of transcribed, genomic loci, including protein-coding genes. As a result, genic transcripts join the secondary piRNA biogenesis loop and are degraded as byproducts of secondary piRNA production. Thus, loss of *Rnf17* results in a cellular autoimmune-like state, where the piRNA machinery, typically directed selectively against transposons, targets protein-coding transcripts, potentially leading to male sterility in adult mice.

## Results

### *Pachytene piRNA cluster organization supports their presumptive role in transposon silencing*

It has been reported that mutations in MIWI affect transposon expression (Reuter et al. 2011). This suggests that pachytene piRNA clusters may produce at least some piRNAs whose role is to suppress transposable elements (TEs). Given that the catalytic activities of MIWI and MILI are important for their function (Reuter et al. 2011; Di Giacomo et al. 2013), it is surprising that a strong

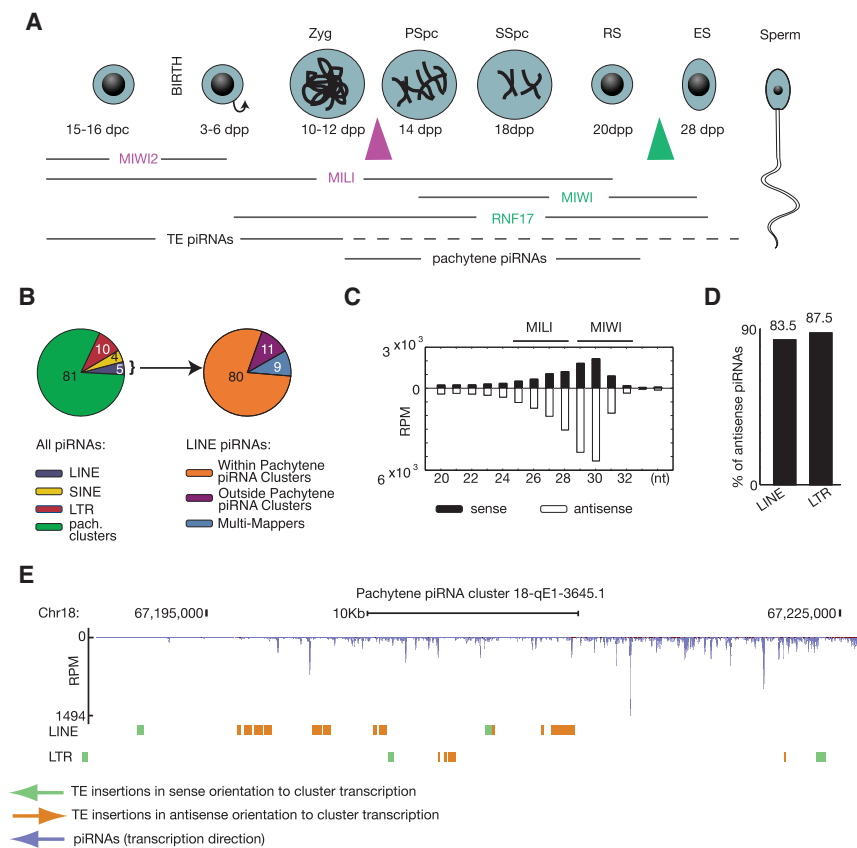


**Figure 1.** Pachytene piRNA clusters are the main source of transposon-derived piRNAs during meiosis. (A) Expression of piRNAs, PIWI proteins, and RNF17 through spermatogenesis. (Zyg) Zygote; (PSpc) pachytene spermatocyte; (SSpc) secondary spermatocyte; (RS) round spermatid; (ES) elongating spermatid. The horizontal lines indicate the window of expression of proteins and piRNAs. Dashed lines indicate reduction of transposon piRNA expression in meiotic cells. Arrowheads demarcate spermatogenesis arrest in *Miw2*<sup>-/-</sup> and/or *Mili*<sup>-/-</sup> (purple) and *Rnf17*<sup>-/-</sup> and/or *Miw1*<sup>-/-</sup> (green) mice. (B) Pie chart summarizing the annotations of piRNA population (24–32 nucleotides [nt]) in adult wild-type testes. LINES were further broken down into classes, which map to different genomic loci: pachytene clusters, outside pachytene clusters, and multimappers. (C) Size profiles of LINE small RNA reads in adult wild-type testes. Sense and antisense orientations to LINES are indicated in black and white, respectively. Horizontal bars indicate the size range of MILI- and MIWI-associated piRNAs. Reads were normalized per million unique genomic mappers (RPM). (D) Percentage of antisense LINE and LTR piRNAs derived from pachytene piRNA clusters that have predominant transposon insertions in one genomic orientation. (E) A genome browser view of piRNAs derived

from a pachytene piRNA cluster at 18-qE1-3645. Transposon insertions oriented sense and antisense with respect to cluster transcription are marked in green and orange, respectively. piRNAs are marked in blue.

ping-pong signature is not seen when such piRNAs engage transposon targets (Beyret et al. 2012). To investigate this inconsistency, we analyzed piRNA populations from whole adult mouse testes, pachytene spermatocytes, and round spermatids, with a focus on LINE-derived piRNAs (LINE piRNAs).

Eighty percent of LINE piRNAs in adult testes emanated from pachytene piRNA clusters. The same was true for piRNAs corresponding to LTR elements and SINEs (Fig. 1B; Supplemental Fig. S1A,B), and a similar observation has been made recently in marmosets (Hirano et al. 2014). This was surprising because pachytene piRNA clusters are generally transposon-poor in comparison with both their adjacent genomic regions (Aravin et al. 2006) and the rest of the genome (Supplemental Fig. S1C). Only a fraction (~25%) of pachytene piRNA clusters gave rise to the vast majority (~96%) of transposon piRNAs. This is true even though those clusters are not enriched for transposon content (Supplemental Fig. S2).

In *Drosophila*, the *flamenco* cluster produces piRNAs that repress transposons in the absence of ping-pong (Brennecke et al. 2007). Transposon insertions into this cluster are overwhelmingly oriented opposite to its unidirectional transcription, producing antisense-enriched piRNA populations. Similarly, a number of pachytene clusters in mice and humans had significant (false discovery rate [FDR] < 0.05) bias for antisense transposon content and produced antisense-biased piRNAs (Fig. 1C–E; Supplemental Fig. S1D; Supplemental Tables S1, S2). This indicates an evolutionary pressure for the production of piRNAs antisense to transposon transcripts. This contrasts with marmosets, in which TE piRNAs derived from pachytene piRNA clusters have no clear bias (Hirano et al. 2014). Support for the function of pachytene piRNA clusters in transposon silencing can be drawn from analysis of a mutation introduced into one such mouse cluster, which resulted in derepression of LINES in adult testes (Xu et al. 2008). Approximately 88% of LINE piRNAs in adult testes exhibited features of primary piRNAs (U at position 1), while a small fraction, 5%, displayed characteristics of secondary piRNAs (A at position 10 and no 1U).

Considered together, the aforementioned findings are consistent with pachytene piRNA clusters playing a role in suppressing transposons during meiosis (Reuter et al. 2011; Di Giacomo et al. 2013). Detection of a small number of secondary piRNAs indicated that MIWI and/or MILI are capable of engaging in the ping-pong cycle in meiotic cells, yet the data suggest limitations on the activity of this arm of the pathway in adult testes.

#### *Rnf17* knockout unleashes ping-pong from transposon-derived piRNAs in adult mice

Previous studies have demonstrated that Tudor proteins act in concert with PIWI proteins (Siomi et al. 2010; Chen et al. 2011). In *Drosophila*, the Tudor protein Qin/Kumo acts as a positive regulator of heterotypic ping-pong between Aubergine and Ago3 (Zhang et al. 2011).

Qin/Kumo has a characteristic structure comprising an E3 ubiquitin ligase domain and five Tudor domains (Supplemental Fig. S3A). This structure is shared by its mouse homolog, RNF17. RNF17 is predominantly expressed in adult testes (Tsutsumi et al. 2012) and interacts physically with MIWI (Vagin et al. 2009). Loss of *Rnf17* produces a phenotype similar to that of a *Miwi* mutant, with arrest in spermatogenesis at the round spermatid stage (Fig. 1A; Supplemental Fig. S3B,C; Deng and Lin 2002; Pan et al. 2005). However, MIWI (or MILI) localization and protein levels are unaffected in *Rnf17*<sup>-/-</sup> mice (Supplemental Fig. S4A–C). Given its role as a positive regulator of ping-pong in flies, we explored the role of RNF17 in the meiotic piRNA pathway in mammals, where its binding partner, MIWI, does not participate in a robust ping-pong cycle (Beyret et al. 2012).

In *Rnf17*<sup>-/-</sup> adult testes and also in isolated secondary spermatocytes and round spermatids, the content of piRNA populations was substantially altered (Fig. 2A; Supplemental Fig. S5A). Overall levels of transposon piRNAs that could be mapped to pachytene piRNA clusters remained unchanged; however, the distribution of transposon piRNAs was dramatically different (Fig. 2A, B; Supplemental Fig. S5A). piRNAs mapping to younger transposon subfamilies (Sookdeo et al. 2013; Molaro et al. 2014) were increased, while other transposon piRNAs were depleted. A reduction was also observed for nontransposon pachytene piRNAs as a whole (Fig. 2A; Supplemental Fig. S5B,C). These changes were most profound in sorted pachytene spermatocytes and round spermatids but were also clearly detectable in small RNAs prepared from whole testes. Such changes were not observed in premeiotic gonads (Fig. 2A,B; Supplemental Fig. S5A). Although testes of *Rnf17* mutant mice differ from wild type in their cellular content, the piRNA phenotype of *Rnf17*<sup>-/-</sup> mice did not appear to be a consequence of shifts in cell type representation resulting from arrested germ cell development. Moreover, the observed phenotype was *Rnf17*-specific. *Miwi*<sup>-/-</sup> or *Tdrd6*<sup>-/-</sup> mice that arrest spermatogenesis at a stage similar to that of *Rnf17*<sup>-/-</sup> (Deng and Lin 2002; Vasileva et al. 2009; Tanaka et al. 2011) failed to show changes in proportions of transposon and nontransposon piRNA populations (Supplemental Fig. S6A–D).

In the *Rnf17* mutant, uniquely mapping LINE piRNAs derived from loci outside pachytene piRNA clusters—i.e., dispersed LINE insertions—exhibited an average 10-fold increase in abundance, and multiply mapping LINE piRNAs showed an average 35-fold increase in abundance (Fig. 2A; Supplemental Fig. S5A). Interestingly, these trends were magnified for piRNAs that map to evolutionarily younger transposon families (Supplemental Fig. S5B,C; Sookdeo et al. 2013; Molaro et al. 2014). While piRNAs corresponding to LINES were the most strongly affected, similar trends were seen for piRNAs corresponding to SINEs and LTR elements (Supplemental Figs. S5C, S7A). Shifts in transposon piRNA abundance were accompanied by changes in piRNA strand bias (Fig. 2C; Supplemental Fig. S7B), with *Rnf17* mutants showing a relative increase in sense piRNAs. This was consistent with an

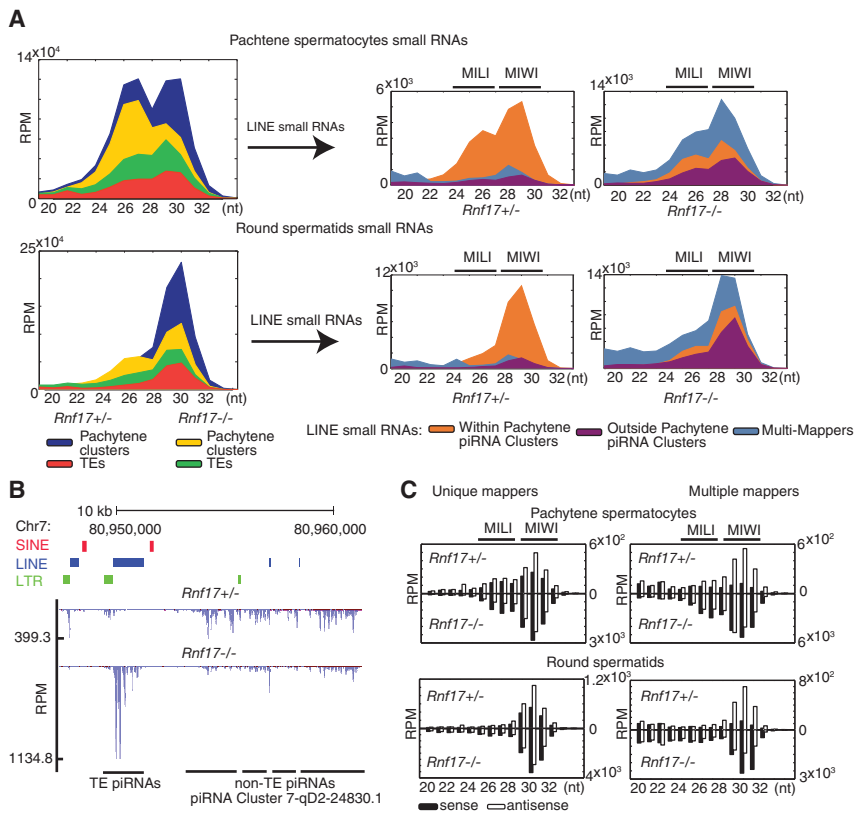


**Figure 2.** *Rnf17* knockout alters the content of piRNA populations. (A) Size profiles of small RNA reads that map to transposon and pachytene piRNA clusters in sorted pachytene spermatocytes and round spermatids of *Rnf17*<sup>+/-</sup> and *Rnf17*<sup>-/-</sup> mice. Reads were normalized per million unique genomic mappers (RPM). The graphs at the right focus on LINE small RNAs (a subset of all transposon piRNAs). All graphs represent an average of three biological replicates. (B) piRNAs mapping to pachytene piRNA cluster 7-qD2-24830.1 in *Rnf17*<sup>+/-</sup> and *Rnf17*<sup>-/-</sup> testes. Black lines indicate transposon- and non-transposon-containing windows of the cluster. Positions of transposons are marked with red (SINE), blue (LINE), or green (LTR). (C) Size profile of LINE small RNA reads mapped to unique and multiple genomic loci in pachytene spermatocytes and round spermatids of *Rnf17*<sup>+/-</sup> and *Rnf17*<sup>-/-</sup> adult mice (note different scales used for +/- and -/- mice). Small RNAs that map in the sense and antisense orientations to LINES are indicated in black and white, respectively. Reads were normalized per million unique genomic mappers (RPM).

activation of cleavage-dependent ping-pong and generation of secondary species from transposon mRNAs. A large proportion of LINE piRNAs in the mutant had an A at position 10 and a 10-nucleotide (nt) overlap with an antisense LINE piRNA (Fig. 3A,B; Supplemental Fig. S7C,D), both characteristics of ping-pong-derived species. Mutation of the fly homolog *qin/kumo* also results in relative increases in sense piRNAs (Zhang et al. 2011). In contrast to *qin/kumo* mutants, where ping-pong is pre-

dominantly homotypic, we observed an increase in both homotypic and heterotypic ping-pong in *Rnf17* mutant testes (Supplemental Fig. S7E). The increase in ping-pong was unlikely to be due to any developmental abnormalities caused by arrested germ cell development because it was not observed in other mutants (*Miwi* or *Tdrd6*) that exhibit developmental arrest at the same stage (Supplemental Fig. S6B,D). Considered together, our data indicate that the loss of *Rnf17* unleashes ping-pong in

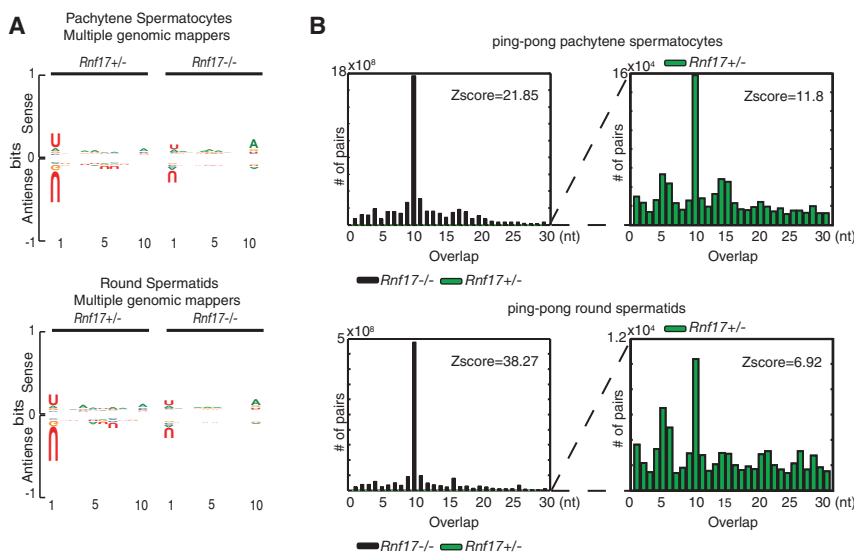


**Figure 3.** *Rnf17* knockout unleashes ping-pong in meiotic cells. (A) Nucleotide distributions (sequence logos) of the first 10 nt of L1 piRNAs for multimappers from sorted pachytene spermatocytes and round spermatids from both *Rnf17*<sup>+/-</sup> and *Rnf17*<sup>-/-</sup> adult mice. (B) The 5'-5' overlap (ping-pong signature) between piRNAs from opposite strands of L1 elements of *Rnf17*<sup>+/-</sup> and *Rnf17*<sup>-/-</sup> sorted pachytene spermatocytes and round spermatids. The number of pairs of piRNA reads at each position is reported. The Z-score was calculated for position 10.

meiotic cells, in effect shifting the meiotic piRNA population toward an embryonic-like state enriched for transposon-derived secondary piRNAs.

*RNF17 associates with piRNA precursors and impacts their selection for further processing*

To investigate the mechanisms by which RNF17 might impact piRNA populations, we examined the levels of piRNA precursors and processing intermediates by surveying RNAs longer than mature piRNAs by RNA sequencing (RNA-seq) and 5' RACE (Supplemental Fig. S8A; Vourekas et al. 2012, 2015). In RNA-seq analysis of RNF17 immunoprecipitates, we noted enrichment in long RNAs mapping to piRNA clusters ( $P < 0.001$ ) (Supplemental Fig. S8B). Additionally, global transcriptional profiles revealed an increase in pachytene cluster transcripts ( $P < 0.001$ ) in *Rnf17*<sup>-/-</sup> testes (Fig. 4A), as was observed in *qin* mutant flies (Zhang et al. 2014). Both results pointed toward RNF17 affecting the flux of precursors into mature piRNAs.

We profiled potential intermediates in piRNA production using RACE to select those long RNAs with 5' monophosphate ends. We compared such species found in association with MILI or MIWI between *Rnf17*<sup>+/-</sup> and *Rnf17* mutant animals and saw changes in representation that paralleled changes in mature small RNA content. Specifically, potential intermediates derived from pachy-

tene cluster transcripts decreased, and those from transposons increased (Fig. 4B; Supplemental Fig. S9A,B). In total RNA, the number of cleaved, 5' monophosphorylated transposon transcripts was unaffected by the *Rnf17* mutation (Fig. 4B; Supplemental Fig. S9A,B), suggesting that, in the mutants, a greater fraction of cleaved transposon RNAs might become associated with PIWI proteins as precursors to piRNA production.

Considered together, our data suggested a role for RNF17 in the selection of precursors for piRNA production (Supplemental Fig. S8A). This could occur by RNF17 directly regulating primary biogenesis. Based on RNA-seq of RNF17 immunoprecipitates, this protein is likely present in the complexes in which precursors are selected. Thus, RNF17 might promote the entry of pachytene cluster transcripts into the biogenesis pathway, while its absence might simply make MILI and MIWI proteins available for ping-pong by reducing the competitive advantage of cluster transcripts. Alternatively, RNF17 might regulate the flux of cluster transcripts into PIWI proteins indirectly. Qin/Kumo has been proposed as an inhibitor of homotypic ping-pong (Zhang et al. 2011). RNF17 could similarly block the ability of MILI and MIWI to play ping-pong. In this way, transposon transcripts would be unable to serve as precursors for piRNA production in the presence of RNF17, leading to nearly exclusive loading of products from pachytene piRNA clusters. In the absence of RNF17, ping-pong would be

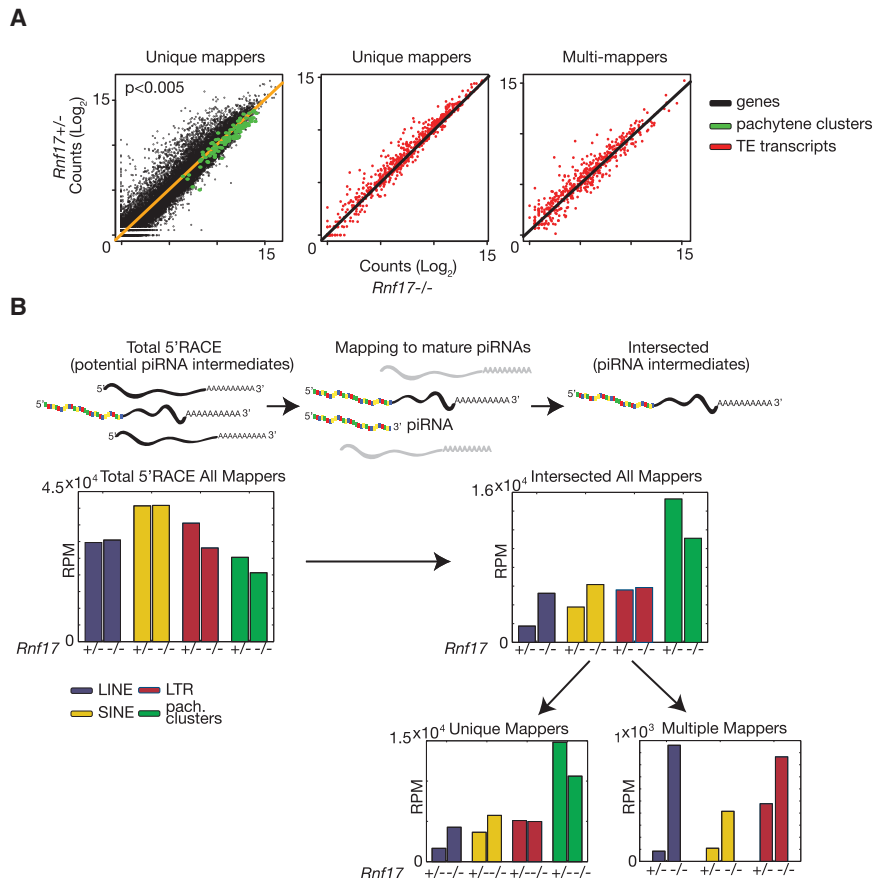


**Figure 4.** RNF17 impacts the selection of piRNA precursors. (A) DESeq analysis of transcript abundance in testes of *Rnf17*<sup>+/-</sup> versus *Rnf17*<sup>-/-</sup> mice. Genes are indicated in black, pachytene piRNA precursors are in green, and transposon transcripts are in red. Axes represent normalized read counts from two independent biological replicates on a log<sub>2</sub> scale. The *P*-value was calculated using Fisher's one-tailed test. (B) The scheme of intersecting the 5' ends of total 5'RACE libraries with mature piRNA sequences (in color) is shown above the bar graphs. The bar graphs display results from 5'RACE analysis from testes of *Rnf17*<sup>+/-</sup> and *Rnf17*<sup>-/-</sup> adult mice. The bar graphs indicate the normalized number of collapsed reads mapping to LINE (blue), SINE (yellow), LTR (red), and pachytene (green) clusters before and after 5' end intersection with sequences of mature piRNAs.

activated, leading to an increased population of MILI and MIWI with transposon piRNAs.

*Genic transcripts harboring fragments of transposons can be drawn into the deregulated piRNA pathway in  $Rnf17^{-/-}$  mice*

Both *Rnf17* and *Miwi* mutants are sterile and show defects in spermatogenesis (Deng and Lin 2002; Pan et al. 2005). However, in *Miwi* mutants, L1 elements were strongly depressed, whereas in *Rnf17* mutants, increased ping-pong led to strengthened repression of transposons (Supplemental Fig. S10A,B). Moreover, while piRNAs from pachytene piRNA clusters were reduced somewhat in *Rnf17* mutants, they were still highly abundant. Thus, it was difficult to rationalize the strong impact of *Rnf17* loss on fertility. We analyzed piRNAs from ~1130 focal sites scattered throughout the genome in *Rnf17^{-/-}* mice (Fig. 5A,B). The majority of those “miniclusters” seen in *Rnf17* mutants were not observed in wild-type mice (Fig. 5A–C). The same sites that gave rise to increased levels of piRNAs also gave rise to increased levels of piRNA processing intermediates (detected in 5' RACE data sets) (Fig. 5C; Supplemental Fig. S10C). All of these “miniclusters” overlapped with transposon-containing regions (Supplemental Fig. S10D). Interestingly, 54% of the miniclusters form within protein-coding genes or long non-coding RNAs (lncRNAs) (Fig. 5D). Clusters formed within protein-coding genes favored SINE subfamilies, while those within lncRNAs or unannotated regions favored LINE subfamilies (Fig. 5E). All de novo clusters in *Rnf17^{-/-}* mice were enriched for evolutionarily younger

and hence more active elements (Fig. 5E; Sookdeo et al. 2013; Molaro et al. 2014).

These observations suggested the possibility that, in the absence of RNF17, protein-coding mRNAs and lncRNAs might be inappropriately targeted by the piRNA pathway simply because they harbor evolutionarily recent transposon insertions. In accord with this hypothesis, *Rnf17* mutants showed a >700-fold increase in ping-pong pairs mapping to protein-coding genes (Fig. 6A). We tested whether transcript cleavage via the ping-pong cycle caused transcript depletion using RNA-seq. Global transcriptional profiles from whole testes identified a number of genes that both harbored de novo miniclusters and showed significant down-regulation in *Rnf17* mutants (Supplemental Table S3; Supplemental Fig. S11A–C). Nine of those genes were pachytene spermatocyte-specific or round spermatid-specific and exhibited a rise in ping-pong pairs from their 3' untranslated regions (UTRs) in the absence of RNF17 (Supplemental Fig. S12A). Of these, *Rnf168* showed the greatest increase in piRNAs (43-fold) upon RNF17 loss. *Rnf168* piRNAs map to a set of SINES in its 3' UTR and show a strong ping-pong signature (Fig. 6B; Supplemental Fig. S12B). Notably, these SINE insertions are not conserved in *Rnf168* homologs in other mammals, suggesting a relatively recent insertion event. Both *Rnf168* and another down-regulated de novo piRNA target, *Tekt4*, are involved in proper progression of spermatogenesis, although, individually, their terminal phenotypes differ from those of RNF17 loss (Roy et al. 2007; Bohgaki et al. 2013).

In an effort to characterize the molecular aspects of the *Rnf17^{-/-}* phenotype further, we prepared RNA-seq

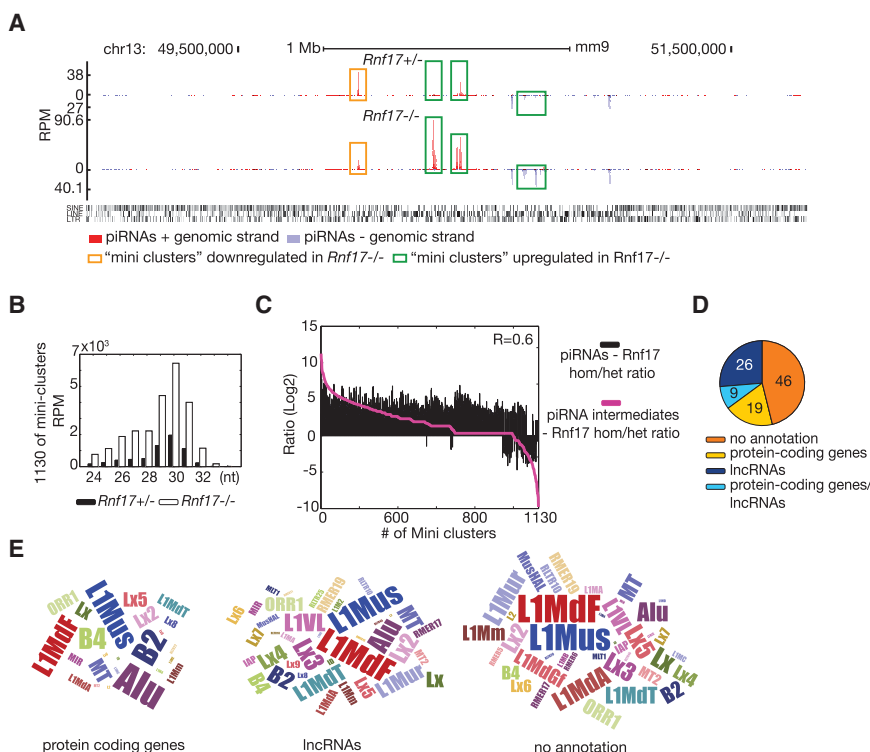


**Figure 5.** piRNAs in *Rnf17^{-/-}* mice arise from multiple genomic loci, including protein-coding genes. (A) A 2-Mb genome browser view of a fragment of chromosome 13 containing four miniclusters. (Orange box) Minicluster down-regulated in *Rnf17^{-/-}*; (green box) minicluster up-regulated in *Rnf17^{-/-}*. piRNA unique mappers derived from + and – genomic strands are shown in red and blue, respectively. (B) Size profile of piRNAs derived from 1130 “miniclusters.” Reads were normalized per million unique genomic mappers (RPM). (C) Log<sub>2</sub> ratio of *Rnf17^{-/-}* to *Rnf17^{+/+}* mature piRNAs (black bars) and piRNA intermediates (pink line) deriving from the 1130 miniclusters. *R* is the coefficient of the correlation. (D) Pie chart summarizing the annotations of piRNA from “miniclusters” that appeared in *Rnf17^{-/-}* testes. Numbers indicate the percent of the total population. (E) Word cloud representing the total length (in base pairs) of different transposon subfamilies in “miniclusters,” separated according to annotation, in *Rnf17^{-/-}* adult testes.

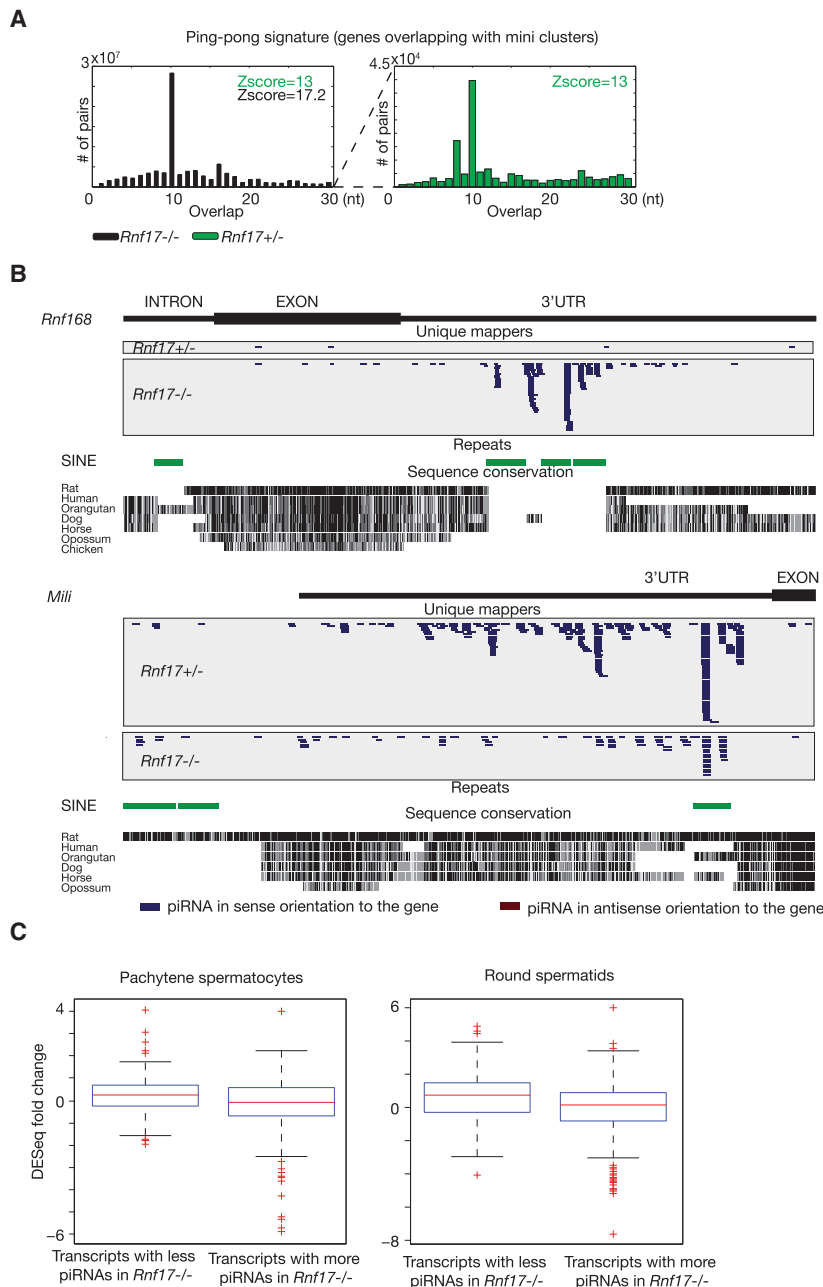


**Figure 6.** RNF17 blocks ping-pong between genic transcripts harboring transposon fragments. (A) The 5'–5' overlap (ping-pong signature) between piRNAs from opposite strands of the 3' UTRs of genes overlapping with piRNA “miniclusters” from testes of *Rnf17<sup>+/-</sup>* and *Rnf17<sup>-/-</sup>* adult mice. The number of pairs of piRNA reads at each position is reported. The Z-score indicates significance of the 10-nt overlap. (B) Genome browser view of piRNAs that uniquely map to a down-regulated gene (*Rnf168*) and an unaffected gene (*Mili*) from testes of *Rnf17<sup>+/-</sup>* and *Rnf17<sup>-/-</sup>* adult mice. (Dark blue) piRNAs in sense orientation to the gene; (dark red) piRNAs in antisense orientation to the gene (none detected). Repeats and conservation are marked for each gene. (C) Box plot representing the expression fold changes of transcripts in *Rnf17<sup>-/-</sup>* versus *Rnf17<sup>+/-</sup>* pachytene spermatocytes and round spermatids in genes that showed a decrease (left) or increase (right) in the level of piRNAs that mapped within their exons. There is a significant difference in the fold changes among the two gene sets; Wilcoxon rank sum  $P$ -value =  $8.2 \times 10^{-6}$  for pachytene spermatocytes,  $P$ -value =  $9.73 \times 10^{-7}$  for round spermatids.

libraries from sorted pachytene spermatocytes and round spermatids from *Rnf17<sup>+/-</sup>* and *Rnf17<sup>-/-</sup>* mice to avoid any confounds due to the mixture of different cells in whole testes. Given that we identified a number of transcripts that become targets of the piRNA pathway and are down-regulated in *Rnf17* mutants, we wished to evaluate whether this observation represented a global trend. We therefore correlated changes in gene expression in *Rnf17<sup>-/-</sup>* pachytene spermatocytes and round spermatids with changes in piRNAs mapping within their transcripts (exons only). Interestingly, there is a significant correlation between genes with less steady-state mRNA in *Rnf17<sup>-/-</sup>* mice and increased numbers of mapping piRNAs. The converse is also true. Genes with fewer map-

ping piRNAs in the mutants showed increased RNA levels (Fig. 6C; Supplemental Table S4). This suggests that a subset of transcripts is targeted by aberrant ping-pong in *Rnf17<sup>-/-</sup>* mice, although the extent to which these changes in gene expression form the underlying basis of the *RNF17<sup>-/-</sup>* sterility phenotype remains to be determined.

## Discussion

Considered together, our data indicate that the ping-pong cycle is actively repressed in meiotic cells and that this requires the Tudor protein RNF17. Loss of RNF17 activates

the ping-pong cycle and redirects the pathway toward younger transposon families as well as protein-coding genes. Although the meiotic piRNA pathway normally disfavors ping-pong, accumulated evidence suggests that it still functions to repress at least some transposons. Moreover, protein-coding genes that harbor insertions of transposon sequence are also down-regulated as a class during spermatogenesis in wild-type animals ( $P < 0.005$ ) (Supplemental Fig. S12C). Thus, perhaps many protein-coding genes are already affected to some extent by the piRNA pathway and may become increasingly ensnared by hyperactivated ping-pong responses in *Rnf17* mutants. This is especially interesting in the context of recent discoveries that a small fraction of mouse pachytene piRNAs actually target protein-coding genes, pseudogenes, and lncRNAs (Goh et al. 2015; Watanabe et al. 2015; Zhang et al. 2015). This observation also suggests that genes strongly expressed at stages when piRNAs are abundant are likely to be under active selection for avoiding transposon insertions. Ping-pong responses are robust during embryonic germ cell development, and this certainly has the potential to consume protein-coding mRNAs with transposon content. The degree to which the activity of ping-pong at these developmental stages would affect RNA levels post-transcriptionally, though, is uncertain. The major outcome of the embryonic piRNA pathway is transcriptional repression, correlating with the deposition of DNA methylation marks (Aravin et al. 2008; Kuramochi-Miyagawa et al. 2008). Methylation within transposon promoters and regulatory elements is essential for their silencing, yet methylation is often observed within the bodies of expressed genes (Lister et al. 2009). Thus, even if the piRNA pathway directs methylation of transposon sequences within introns or 3' UTRs, these marks may be largely irrelevant to the activity of gene promoters.

Our data could suggest that the sterility of *Rnf17* mutant animals results at least in part from the cumulative depletion of one or more coding or noncoding transcript via a piRNA-based autoimmune mechanism. Among the transcripts that were down-regulated and had increased numbers of piRNA mappers in *Rnf17*<sup>-/-</sup> mice (Fig. 6C; Supplemental Table S4) we found a helicase, transcription factors, translation initiation factors, phosphatases, and many proteins that generally regulate the cell cycle in different manners (Supplemental Table S4). This depletion of transcripts is potentially necessary for meiotic division, or proper progression of spermatogenesis could certainly cause a cascade of secondary effects resulting in arrested germ cell development. One such effect is down-regulation of protamines (*Prm1* and *Prm2*) and transition proteins (*Tnp1* and *Tnp2*) required for round spermatid nucleus elongation and might partially explain the arrest at the round spermatid stage (Supplemental Table S5).

Recently, it was shown that secondary piRNAs initiate the spreading of primary piRNA production along the precursor transcripts (Mohn et al. 2015; Zhang et al. 2015). In light of these data, it is possible that even a single, secondary piRNA could lead to a burst of piRNA production from the targeted locus. This finding supports a crucial role of

RNF17 in the suppression of ping-pong during mouse meiosis.

In wild-type testes piRNAs target a number of genic transcripts during adult spermatogenesis, and this targeting is most likely required for proper progression of spermatogenesis (Goh et al. 2015; Watanabe et al. 2015; Zhang et al. 2015). In our data sets, we identified many genes that had fewer piRNAs in *Rnf17*<sup>-/-</sup> testes with a corresponding increase in transcript abundance (Fig. 6C; Supplemental Table S4). Interestingly, the most up-regulated transcript in *Rnf17*<sup>-/-</sup> pachytene spermatocytes was *Preli1* (Supplemental Table S4). *Preli1* mRNA contains MIR and LINE2 sequences and is targeted by piRNAs during spermatogenesis in wild-type testes (Watanabe et al. 2015). MIR- and LINE2-derived piRNAs go down in *Rnf17*<sup>-/-</sup> mice (Supplemental Fig. 5B,C), as do piRNAs mapping to *Preli1* transcript (the ratio of *Rnf17*<sup>-/-</sup>: *Rnf17*<sup>+/+</sup> piRNAs mapping to *Preli1* was 0.02). Perhaps, since MIR and LINE2 are not evolutionarily young transposon families, those types of transposons do not present sufficient amounts of sense and antisense RNA to fuel the ping-pong cycle. This raises an alternative explanation of the *Rnf17*<sup>-/-</sup> phenotype in which we hypothesize that the shift of MIWI and MILI away from binding canonical piRNA populations might cause sterility, just as loss of MIWI does, for example. It should be noted, however, that meiotic piRNA populations are still relatively abundant (approximately half of wild type) in the *Rnf17* mutants despite the activation of the ping-pong cycle.

Overall, our study demonstrates that the protein components of the meiotic piRNA pathway are perfectly capable of engaging in the ping-pong cycle but that this is normally actively repressed. Suppression of ping-pong presumably protects protein-coding genes, fully one-quarter of which contain transposon-derived sequences, from being silenced by the pathway, preserving the expression of genes essential for spermatogenesis.

## Materials and methods

### Mice

*Rnf17* knockout mice were generously provided by Jeremy Wang (Pan et al. 2005). *Miwi* knockout mice were generously provided by Haifan Lin (Deng and Lin 2002). All mice were maintained according to the guidelines of the Cold Spring Harbor Laboratory Institutional Animal Care and Use Committee.

### Germ cell isolation and purification by fluorescence-activated cell sorting

Germ cells were isolated and purified according to a previously published protocol (Bastos et al. 2005) with minor modifications. Briefly, testes were isolated from one adult mouse for each sorting experiment, and the tunica was removed. Tissue was digested for 45 min at 37°C in a dissociation buffer containing 25 mg of collagenase A (Roche), 25 mg of Dispase II (Life Technologies), and 2.5 mg of DNase I (Roche). Cell suspensions diluted to  $1 \times 10^6$  cells per milliliter were then stained with Hoechst 33342 (Sigma, H3570) at a concentration of 5 mg/mL for 30 min at 37°C in HBSS buffer, 25 mM Hepes, 1.5 mM EDTA, and 5% FBS (HBSS<sup>+</sup>). Cells

were then washed and stained with Ep-CAM antibody conjugated with Alexa fluor 647 (Biolegend, clone G8.8) for 30 min on ice. Cells were then washed in HBSS<sup>+</sup> and resuspended at a concentration of  $10 \times 10^6$  cells per milliliter in HBSS<sup>+</sup>. Immediately before analysis, 1 mg/mL propidium iodide was added for dead cell exclusion. Analysis was performed in a five-laser Aria II cell sorter (Becton Dickinson). Hoechst was excited with a UV laser at 350 nm, and fluorescence was recorded with a 450/50 filter (Hoechst Blue) and 670LP filter (Hoechst Red). A 505LP filter was used to separate the emission wavelengths. Pachytene spermatocytes and round spermatids were gated based on their Hoechst Blue-Red profile in scatter plots as well as Hoechst Blue fluorescence and forward and side scatter properties. Diploid spermatogonia were gated based on their Hoechst Blue-Red profile and further distinguished from somatic cells based on EpCAM staining. After applying gates, cells were plated directly into Trizol (Invitrogen) for RNA isolation.

#### *Immunofluorescence, RNA immunoprecipitation, and Western blot*

For immunofluorescence, mouse testes were dissected in 1× PBS and fixed in fresh 4% PFA (in 1× PBS) for 2–3 h at 4°C and then washed twice with 50% ethanol and twice with 70% ethanol for 30 min each. After fixation, samples were embedded in OCT blocks and cut at 5- $\mu$ m slices. Paraffin was removed with HistoClear (National Diagnostics), and slices were washed with 1× PBS, blocked with 10% goat serum (in 1× PBS) for 30 min, incubated with primary antibodies (1:500) overnight at 4°C, washed three times with 1× TBST for 10 min each, and incubated with secondary antibodies (1:1000) for 1 h at room temperature. The slices were then washed twice with 1× TBST and incubated with DAPI (1:10000 in 1× PBS) for 5 min, washed twice for 10 min each with 1× PBS, and mounted using ProLong Gold anti-fade reagent (Invitrogen, P36930). Images were acquired with a Zeiss 710 LSM confocal microscope. The primary antibodies used were rabbit L1-ORF antibody (a kind gift from Alex Bortvin) (Soper et al. 2008), mouse phospho-Histone H2A.X (Millipore, 05-636), SCP3 (Abcam), mouse MILI (Santa Cruz Biotechnology), and rabbit TDRD6 (Hosokawa et al. 2007). The secondary fluorescent antibodies (Invitrogen) used were goat anti-rabbit IgG Alexa fluor 488 (A11008) and goat anti-mouse IgG Alexa fluor 546 (A21043). RNA immunoprecipitations and Western blots were done as previously described (Aravin et al. 2008; Vagin et al. 2013); we used rabbit RNF17 1774 antibody (Pan et al. 2005), rabbit MIWI-N2 antibody, rabbit MILI antibody (Vagin et al. 2009), and Tubuline antibody (Sigma, T6074).

#### *Small RNA, transcriptome, and global 5'RACE library preparation*

Small RNA and NSR transcriptome libraries were prepared as previously described (Armour et al. 2009; Malone et al. 2012). Transcriptome libraries from sorted pachytene spermatocytes and round spermatids were prepared using Ovation RNA-seq system version 2 (Nugen) according to manufacturer's instructions. Global 5'RACE libraries were prepared from total testes or MIWI/MILI immunoprecipitations as previously described (Karginov et al. 2010). Material was obtained from testes or sorted cells of sibling adult (6- to 10-wk-old) *Rnf17*<sup>-/-</sup> and *Rnf17*<sup>+/-</sup> mice.

#### *Sequencing, mapping, and annotation*

Small RNA libraries were run on an Illumina Genome Analyzer II (single end 36). After removing adapters, small RNA reads were

first mapped to the mm9 mouse genome with Bowtie (Langmead et al. 2009), with up to two mismatches and a maximum of 100 multiple alignments (otherwise suppressed). Unmapped reads were remapped using STAR (Dobin et al. 2013) with the same criteria in order to extract spliced reads. Transcriptome and 5'RACE libraries were run on an Illumina Genome Analyzer II or MiSeq (single end 76 or single end 101). NSR transcriptome libraries were reverse-complemented and trimmed (removing the first 8 nt). They were then mapped to the mm9 mouse genome with STAR (allowing two mismatches and a maximum of 100 multiple alignments). 5'RACE libraries were mapped to the mm9 mouse genome with STAR (allowing two mismatches and a maximum of 100 multiple alignments).

All reads were annotated based on genomic locations against structural RNAs (University of California at Santa Cruz [UCSC] RepeatMasker track), microRNA (miRNA) (miRBase 18), TEs (UCSC RepeatMasker track), 214 pachytene piRNA cluster coordinates (Li et al. 2013), RefSeq genes (UCSC RefSeq track), and testis-specific lncRNAs (Liu et al. 2011; Sun et al. 2013). At least 50% of the read was required to overlap with the feature before being assigned an annotation.

#### *Transcriptome analysis*

Reads mapped to structural RNAs and miRNAs were removed from each library. The rest of the reads were assigned to TEs, pachytene piRNA clusters, and genes. For genes and pachytene piRNA clusters, only uniquely mapped reads were used for downstream analysis. Expression abundance estimation was performed for genes and pachytene piRNA clusters using the HTSeq count script available in the HTSeq Python framework (Anders et al. 2015). For TEs, uniquely and multiply mapped reads were used separately for downstream analysis and counted using BEDTools (Quinlan and Hall 2010). Differential expression analysis was performed using the DESeq (Anders and Huber 2010) package available in R/Bioconductor. Reads were normalized based on an internally calculated "size factor" in DESeq. Biological replicates were averaged and converted into a log<sub>2</sub> transformed scale. Linear regression was then estimated between libraries by fitting a linear model in R. The numbers of data points above and below the regression line from genes, pachytene piRNA clusters, and TEs were counted, and a one-tail Fisher's statistic was calculated to obtain *P*-values. All plots were generated in R. The numbers of replicates used from *Rnf17*<sup>+/-</sup> and *Rnf17*<sup>-/-</sup> mice were three pachytene spermatocytes, three round spermatids, and three whole testes.

#### *Small RNA library analysis*

In order to create the averaged graphs of small RNA libraries, reads from independent biological replicates were summed up and normalized with a sum of total unique genomic mappers (excluding structural RNA). The numbers of replicates used from *Rnf17*<sup>+/-</sup> and *Rnf17*<sup>-/-</sup> mice were two gonads, three pachytene spermatocytes, three round spermatids, and two whole testes. *Miwi*<sup>+/-</sup>, *Miwi*<sup>-/-</sup>, *Tdrd6*<sup>+/-</sup>, and *Tdrd6*<sup>-/-</sup> libraries had no replicates.

#### *5'RACE analysis*

Only RACE reads >40 nt were analyzed in order to avoid potential contamination from mature piRNAs. To assess intersections/overlaps between the 5'RACE and small RNA libraries, the 5' genomic position of each read was compared with the unique 5' genomic position of all mature piRNA reads (24–31 nt) to identify shared 5' ends, indicative of intersection.

Wasik et al.

### Sequence logos

In order to generate nucleotide distributions (sequence logos), reads matching the desired criteria were separated into unique mappers or multimappers and based on their orientation to desired features. The logos were generated with Weblogo3 (Crooks et al. 2004).

### Ping-pong analysis

We determined the ping-pong signature using the tool generously provided by Phil Zamore (Li et al. 2013). For assessing a ping-pong signal of L1 elements, we mapped small RNA reads to an L1 consensus sequence (L1D84391) with two mismatches. For assessing ping-pong signals in mini-piRNA clusters, we mapped all small RNA reads to the minicluster coordinates with two mismatches. We then assessed ping-pong signals of uniquely mapped reads oriented sense to miniclusters against all reads oriented antisense. We then normalized antisense ping-pong contribution by the number of miniclusters to which the antisense read mapped. The mapped results were then processed to provide the strength of ping-pong pairs at each offset. A “Z-score” was calculated using  $Z = (P10-A)/S$ , where P10 is the value at offset 10, and A and S are the mean and standard deviation, respectively, of values at offsets 1–9 and 11–30.

In order to count homotypic and heterotypic ping-pong pairs, we analyzed MIWI and MILI small RNA immunoprecipitation libraries. First, we counted the total number of pairs with 10-nt 5' end overlap present within each immunoprecipitation library. These pairs can perform homotypic ping-pong. We then counted the number of pairs with 10-nt 5' end overlap across MIWI and MILI immunoprecipitations (excluding the pairs that were counted as homotypic) and treated them as heterotypic ping-pong substrates. Importantly, since the majority of MIWI- and MILI-associated piRNAs share their 5' ends, many of the theoretically homotypic ping-pong pairs can in fact be heterotypic. The number of homotypic ping-pong pairs was normalized with total number of unique mappers for each immunoprecipitation. The number of heterotypic pairs was normalized with the sum of unique mappers from both immunoprecipitations.

### Identification of miniclusters

Using the guidelines described previously (Aravin et al. 2006), we searched for the presence of de novo piRNA clusters in wild-type and *Rnf17* mutant testes. In brief, a series of sliding windows were generated from the mouse genome using BEDTools, each 1 kb in size and having 900 base pairs (bp) overlapping with adjacent windows. Sliding windows that overlap previously annotated piRNA clusters were removed from subsequent analyses. Coverage of each sliding window was calculated from small RNA libraries generated from whole wild-type or *Rnf17* mutant testes using only reads that are uniquely mapped and at least 24 nt in length. Windows with a coverage less than three piRNA reads per kilobase were discarded. Differential analyses performed using DESeq identified sliding windows that show differential expression (FDR < 0.05) between heterozygous mice and *Rnf17* mutants, which were merged into larger intervals if they were overlapping or bookended. The coordinates were further refined by the position of the outermost piRNA in each region.

### Measuring transposon content in pachytene clusters

We counted total transposon length (total number of base pairs covered) within prepachytene and pachytene piRNA clusters (Li et al. 2013) and the length of the genomic intervals between the

piRNA clusters using BEDTools (Intersect). Transposon coordinates were obtained from the RepeatMasker track from UCSC. We calculated the average percent of transposon content in those three classes of intervals and compared them using the Wilcoxon rank sum test.

### Identification of the pachytene piRNA clusters with genomic transposon insertion bias

We filtered for clusters that were at least 20 kb or longer and had at least two insertions of LINES, LTRs, or SINEs. Orientation of transposon instance/insertion was determined relative to genomic strand, and the proportion of transposon inserted on the plus (+) and minus (–) strands was calculated. A permutation test was performed in which 100-kb genomic regions were randomly selected that do not overlap piRNA clusters, and the relative orientation bias (proportion) was calculated. piRNA clusters were then compared with the permutation data set to obtain an empirical *P*-value, corrected for multiple testing using Benjamini-Hochberg (FDR).

### Word cloud

We calculated total transposon length in three groups of piRNA miniclusters (in protein-coding genes, lncRNAs, and areas with no annotation) for known transposon subfamilies. We represented total length of a subfamily with the number of words equal to the number of base pairs that this subfamily occupies within the piRNA miniclusters. The words served as input for the word cloud generator (<https://www.jasondavies.com/wordcloud/>).

### Genic transcript level comparison before and during meiosis

We compared transcript levels between 10.5 d post-partum (dpp; P10, before meiosis) and 17.5 dpp (P17, start of meiosis) from publicly available transcriptome data sets (Li et al. 2013). All transcripts for which at least one transposon was identified as being fully enveloped in its 3' UTR were identified using intersectBed (BEDTools). Following this, the  $\log_2$  (P10/P17) values of FPKM (fragments per kilobase per million mapped fragments) values were compared between transcripts harboring at least one transposon versus no transposon in the 3' UTR.

### Correlation of gene transcription and piRNA targeting

The current (May 30, 2015) mm9 RefSeq GTF file was obtained from UCSC genome browser. All gene entries were collapsed using BEDTools “merge” to develop a BED file of nonoverlapping genomic intervals. Using this BED file, a fasta file was generated using BED tool “get fasta,” and this was then transformed into a Bowtie index. Sequencing reads (three replicates of each library) from pachytene spermatocytes and round spermatids of *Rnf17<sup>+/-</sup>* and *Rnf17<sup>-/-</sup>* mice were trimmed of their adapters using FASTX\_clipper. Files were filtered for reads 24–32 nt long. Reads were then aligned with no mismatches and no maximum on the number of alignments allowed. Mapped counts were then normalized using DESeq. Genes were identified where either one of the *Rnf17<sup>+/-</sup>* or *Rnf17<sup>-/-</sup>* library had an average of 10 piRNA reads mapped per million and the  $\log_2$  fold changes were in either the top or bottom quintile. These genes were then compared for their RNA-seq expression fold changes (described above). In the case of both pachytene spermatocytes and round spermatids, there was a significant difference in the fold changes among the two gene sets; Wilcoxon Rank-Sum *P*-value =  $8.2 \times 10^{-6}$  for pachytene spermatocytes, and *P*-value =  $9.73 \times 10^{-7}$  for round spermatids.

*Quantitative RT-PCR (qRT-PCR) for the genes that harbor piRNA miniclusters*

RNA was extracted using TRIzol reagent (Invitrogen) according to the manufacturers' instructions. RNA was treated with DNase I amplification grade (Invitrogen). Complementary DNA was prepared by reverse transcription using oligo(dT)20 primer and SuperScript III reverse transcriptase (Invitrogen). qPCR was carried out using SYBR Green PCR master mix (Invitrogen) on a Chromo4 real-time PCR detector (Bio-Rad). Transcripts were quantified using the  $\Delta\Delta C_T$  method (Livak and Schmittgen 2001) and normalized to transcript levels of a reference gene (*Mvh* or *Actb*). At least two biological replicates were used to measure the gene expression. We used the following primers: *Rnf168-f* (CAAGAAGAGCAGGACAGATTGTT) and *Rnf168-r* (GGGTGTGCGTAGCTGGTACT), *Spata9-f* (TCCTGCCAACCAAGCAGAGTA) and *Spata9-r* (TCCCTACCCTGTCCCTTCTT), *Spatc1-f* (AGTTGGATGAGGACCTGTGC) and *Spatc1-r* (TAGCACACGCTGCAAGAAGT), *Tekt4-f* (CGAGGTGGAGGAGTTGAACA) and *Tekt4-r* (GCGGTGGGTGCATACACTTCT), *GM597-f* (TGATCTTGTCCGAGGCTCT) and *GM597-r* (AATCAGTGGAGGCATTCCAG), *Mvh-f* (AAAGAAATCGCTCTGCCAGT) and *Mvh-r* (ATTTTCGCTGTGGAAGTGC), *Rnf17-f* (CCCTCAAGAAAATGAAGATGGA) and *Rnf17-r* (GGCTGCTTCTTTTCCCTTC), *Miwi-f* (AGTGAGAAGCGGGAGTGTGT) and *Miwi-r* (CACGTGGCAGAGCTTGATG), and *Actb-f* (CGTTCCGATGCCCTGAGGCTCTT) and *Actb-r* (CGTCACTTTCATGATGGAATTGA).

Primary sequencing data can be obtained from the Gene Expression Omnibus (GSE53919 and GSE17319).

## Acknowledgments

We are grateful to Phil Zamore and Bo Han for providing pachytene piRNA cluster coordinates and ping-pong analysis tools, Jeremy Wang for sharing *Rnf17* knockout mice and RNF17 antibodies, and Alex Bortvin for sharing L1 ORF1 antibodies. We are grateful to Ian Peikon for critical reading of the manuscript. We thank the Bioinformatics Shared Resource at Cold Spring Harbor Laboratory for help with data analysis. We thank Emily Lee, Elena Ghiban, Laura Cardone, and Danae Rebboline for assistance with Illumina sequencing. G.J.H. is an investigator of the Howard Hughes Medical Institute. K.A.W. is a George A. and Marjorie H. Anderson Fellow of the Watson School of Biological Sciences. O.H.T. is supported by a fellowship from the Human Frontier Science Program. This work was supported by a generous gift from Kathryn W. Davis and a grant from the National Institutes of Health (5R01GM062534). K.A.W., V.V.V., and G.J.H. designed the experiments and wrote the manuscript. K.A.W., I.F., and V.V.V. performed the experiments. K.A.W., O.H.T., V.V.V., S.R.K., and M.H. performed the data analysis.

## References

Anders S, Huber W. 2010. Differential expression analysis for sequence count data. *Genome Biol* **11**: R106.  
 Anders S, Pyl PT, Huber W. 2015. HTSeq—a Python framework to work with high-throughput sequencing data. *Bioinformatics* **31**: 166–169.  
 Aravin AA, Hannon GJ. 2008. Small RNA silencing pathways in germ and stem cells. *Cold Spring Harb Symp Quant Biol* **73**: 283–290.  
 Aravin A, Gaidatzis D, Pfeffer S, Lagos-Quintana M, Landgraf P, Iovino N, Morris P, Brownstein MJ, Kuramochi-Miyagawa S,

Nakano T, et al. 2006. A novel class of small RNAs bind to MILI protein in mouse testes. *Nature* **442**: 203–207.  
 Aravin AA, Hannon GJ, Brennecke J. 2007. The Piwi-piRNA pathway provides an adaptive defense in the transposon arms race. *Science* **318**: 761–764.  
 Aravin AA, Sachidanandam R, Bourc'his D, Schaefer C, Pezic D, Toth KF, Bestor T, Hannon GJ. 2008. A piRNA pathway primed by individual transposons is linked to de novo DNA methylation in mice. *Mol Cell* **31**: 785–799.  
 Armour CD, Castle JC, Chen R, Babak T, Loerch P, Jackson S, Shah JK, Dey J, Rohl CA, Johnson JM, et al. 2009. Digital transcriptome profiling using selective hexamer priming for cDNA synthesis. *Nat Methods* **6**: 647–649.  
 Bao J, Yan W. 2012. Male germline control of transposable elements. *Biol Reprod* **86**: 162, 161–114.  
 Bastos H, Lassalle B, Chicheportiche A, Riou L, Testart J, Allemand I, Fouchet P. 2005. Flow cytometric characterization of viable meiotic and postmeiotic cells by Hoechst 33342 in mouse spermatogenesis. *Cytometry A* **65**: 40–49.  
 Beyret E, Liu N, Lin H. 2012. piRNA biogenesis during adult spermatogenesis in mice is independent of the ping-pong mechanism. *Cell Res* **22**: 1429–1439.  
 Bohgaki M, Bohgaki T, El Ghamrasni S, Srikumar T, Maire G, Panier S, Fradet-Turcotte A, Stewart GS, Raught B, Hakem A, et al. 2013. RNF168 ubiquitylates 53BP1 and controls its response to DNA double-strand breaks. *Proc Natl Acad Sci* **110**: 20982–20987.  
 Brennecke J, Aravin AA, Stark A, Dus M, Kellis M, Sachidanandam R, Hannon GJ. 2007. Discrete small RNA-generating loci as master regulators of transposon activity in *Drosophila*. *Cell* **128**: 1089–1103.  
 Carmell MA, Girard A, van de Kant HJ, Bourc'his D, Bestor TH, de Rooij DG, Hannon GJ. 2007. MIWI2 is essential for spermatogenesis and repression of transposons in the mouse germline. *Dev Cell* **12**: 503–514.  
 Castaneda J, Genzor P, Bortvin A. 2011. piRNAs, transposon silencing, and germline genome integrity. *Mutat Res* **714**: 95–104.  
 Chen C, Nott TJ, Jin J, Pawson T. 2011. Deciphering arginine methylation: Tudor tells the tale. *Nat Rev Mol Cell Biol* **12**: 629–642.  
 Chuma S, Nakano T. 2013. piRNA and spermatogenesis in mice. *Philos Trans R Soc Lond B Biol Sci* **368**: 20110338.  
 Crooks GE, Hon G, Chandonia JM, Brenner SE. 2004. WebLogo: a sequence logo generator. *Genome Res* **14**: 1188–1190.  
 Deng W, Lin H. 2002. miwi, a murine homolog of piwi, encodes a cytoplasmic protein essential for spermatogenesis. *Dev Cell* **2**: 819–830.  
 Di Giacomo M, Comazzetto S, Saini H, De Fazio S, Carrieri C, Morgan M, Vasiliauskaite L, Benes V, Enright AJ, O'Carroll D. 2013. Multiple epigenetic mechanisms and the piRNA pathway enforce LINE1 silencing during adult spermatogenesis. *Mol Cell* **50**: 601–608.  
 Dobin A, Davis CA, Schlesinger F, Drenkow J, Zaleski C, Jha S, Batut P, Chaisson M, Gingeras TR. 2013. STAR: ultrafast universal RNA-seq aligner. *Bioinformatics* **29**: 15–21.  
 Girard A, Sachidanandam R, Hannon GJ, Carmell MA. 2006. A germline-specific class of small RNAs binds mammalian Piwi proteins. *Nature* **442**: 199–202.  
 Goh WS, Falcatori I, Tam OH, Burgess R, Meikar O, Kotaja N, Hammell M, Hannon GJ. 2015. piRNA-directed cleavage of meiotic transcripts regulates spermatogenesis. *Genes Dev* **29**: 1032–1044.  
 Hirano T, Iwasaki YW, Lin ZY, Imamura M, Seki NM, Sasaki E, Saito K, Okano H, Siomi MC, Siomi H. 2014. Small RNA

- profiling and characterization of piRNA clusters in the adult testes of the common marmoset, a model primate. *RNA* **20**: 1223–1237.
- Hosokawa M, Shoji M, Kitamura K, Tanaka T, Noce T, Chuma S, Nakatsuji N. 2007. Tudor-related proteins TDRD1/MTR-1, TDRD6 and TDRD7/TRAP: domain composition, intracellular localization, and function in male germ cells in mice. *Dev Biol* **301**: 38–52.
- Karginov FV, Cheloufi S, Chong MM, Stark A, Smith AD, Hannon GJ. 2010. Diverse endonucleolytic cleavage sites in the mammalian transcriptome depend upon microRNAs, Drosha, and additional nucleases. *Mol Cell* **38**: 781–788.
- Klattenhoff C, Theurkauf W. 2008. Biogenesis and germline functions of piRNAs. *Development* **135**: 3–9.
- Kota SK, Feil R. 2010. Epigenetic transitions in germ cell development and meiosis. *Dev Cell* **19**: 675–686.
- Kuramochi-Miyagawa S, Kimura T, Ijiri TW, Isobe T, Asada N, Fujita Y, Ikawa M, Iwai N, Okabe M, Deng W, et al. 2004. Mili, a mammalian member of piwi family gene, is essential for spermatogenesis. *Development* **131**: 839–849.
- Kuramochi-Miyagawa S, Watanabe T, Gotoh K, Totoki Y, Toyoda A, Ikawa M, Asada N, Kojima K, Yamaguchi Y, Ijiri TW, et al. 2008. DNA methylation of retrotransposon genes is regulated by Piwi family members MILI and MIWI2 in murine fetal testes. *Genes Dev* **22**: 908–917.
- Langmead B, Trapnell C, Pop M, Salzberg SL. 2009. Ultrafast and memory-efficient alignment of short DNA sequences to the human genome. *Genome Biol* **10**: R25.
- Lau NC, Seto AG, Kim J, Kuramochi-Miyagawa S, Nakano T, Bartel DP, Kingston RE. 2006. Characterization of the piRNA complex from rat testes. *Science* **313**: 363–367.
- Li XZ, Roy CK, Dong X, Bolcun-Filas E, Wang J, Han BW, Xu J, Moore MJ, Schimenti JC, Weng Z, et al. 2013. An ancient transcription factor initiates the burst of piRNA production during early meiosis in mouse testes. *Mol Cell* **50**: 67–81.
- Lister R, Pelizzola M, Dowen RH, Hawkins RD, Hon G, Tonti-Filippini J, Nery JR, Lee L, Ye Z, Ngo QM, et al. 2009. Human DNA methylomes at base resolution show widespread epigenomic differences. *Nature* **462**: 315–322.
- Liu W, Zhao Y, Cui P, Lin Q, Ding F, Xin C, Tan X, Song S, Yu J, Hu S. 2011. Thousands of novel transcripts identified in mouse cerebrum, testis, and ES cells based on ribo-minus RNA sequencing. *Front Genet* **2**: 93.
- Livak KJ, Schmittgen TD. 2001. Analysis of relative gene expression data using real-time quantitative PCR and the  $2^{-\Delta\Delta C_T}$  method. *Methods* **25**: 402–408.
- Malone CD, Hannon GJ. 2009. Small RNAs as guardians of the genome. *Cell* **136**: 656–668.
- Malone C, Brennecke J, Czech B, Aravin A, Hannon GJ. 2012. Preparation of small RNA libraries for high-throughput sequencing. *Cold Spring Harb Protoc* **2012**: 1067–1077.
- Mohn F, Handler D, Brennecke J. 2015. Noncoding RNA. piRNA-guided slicing specifies transcripts for Zucchini-dependent, phased piRNA biogenesis. *Science* **348**: 812–817.
- Molaro A, Falciatori I, Hodges E, Aravin AA, Marran K, Rafii S, McCombie WR, Smith AD, Hannon GJ. 2014. Two waves of de novo methylation during mouse germ cell development. *Genes Dev* **28**: 1544–1549.
- Pan J, Goodheart M, Chuma S, Nakatsuji N, Page DC, Wang PJ. 2005. RNF17, a component of the mammalian germ cell nuage, is essential for spermiogenesis. *Development* **132**: 4029–4039.
- Pillai RS, Chuma S. 2012. piRNAs and their involvement in male germline development in mice. *Dev Growth Differ* **54**: 78–92.
- Quinlan AR, Hall IM. 2010. BEDTools: a flexible suite of utilities for comparing genomic features. *Bioinformatics* **26**: 841–842.
- Reuter M, Berninger P, Chuma S, Shah H, Hosokawa M, Funaya C, Antony C, Sachidanandam R, Pillai RS. 2011. Miwi catalysis is required for piRNA amplification-independent LINE1 transposon silencing. *Nature* **480**: 264–267.
- Roy A, Lin YN, Agno JE, DeMayo FJ, Matzuk MM. 2007. Absence of tektin 4 causes asthenozoospermia and subfertility in male mice. *FASEB J* **21**: 1013–1025.
- Siomi MC, Mannen T, Siomi H. 2010. How does the royal family of Tudor rule the PIWI-interacting RNA pathway? *Genes Dev* **24**: 636–646.
- Siomi MC, Sato K, Pezic D, Aravin AA. 2011. PIWI-interacting small RNAs: the vanguard of genome defence. *Nat Rev Mol Cell Biol* **12**: 246–258.
- Sookdeo A, Hepp CM, McClure MA, Boissinot S. 2013. Revisiting the evolution of mouse LINE-1 in the genomic era. *Mob DNA* **4**: 3.
- Soper SF, van der Heijden GW, Hardiman TC, Goodheart M, Martin SL, de Boer P, Bortvin A. 2008. Mouse maelstrom, a component of nuage, is essential for spermatogenesis and transposon repression in meiosis. *Dev Cell* **15**: 285–297.
- Sun J, Lin Y, Wu J. 2013. Long non-coding RNA expression profiling of mouse testis during postnatal development. *PLoS One* **8**: e75750.
- Tanaka T, Hosokawa M, Vagin VV, Reuter M, Hayashi E, Mochizuki AL, Kitamura K, Yamanaka H, Kondoh G, Okawa K, et al. 2011. Tudor domain containing 7 (Tdrd7) is essential for dynamic ribonucleoprotein (RNP) remodeling of chromatoid bodies during spermatogenesis. *Proc Natl Acad Sci* **108**: 10579–10584.
- Tsutsumi M, Kowa-Sugiyama H, Bolor H, Kogo H, Inagaki H, Ohye T, Yamada K, Taniguchi-Ikeda M, Toda T, Kurahashi H. 2012. Screening of genes involved in chromosome segregation during meiosis I: in vitro gene transfer to mouse fetal oocytes. *J Hum Genet* **57**: 515–522.
- Vagin VV, Wohlschlegel J, Qu J, Jonsson Z, Huang X, Chuma S, Girard A, Sachidanandam R, Hannon GJ, Aravin AA. 2009. Proteomic analysis of murine Piwi proteins reveals a role for arginine methylation in specifying interaction with Tudor family members. *Genes Dev* **23**: 1749–1762.
- Vagin VV, Yu Y, Jankowska A, Luo Y, Wasik KA, Malone CD, Harrison E, Rosebrock A, Wakimoto BT, Fagegaltier D, et al. 2013. Minotaur is critical for primary piRNA biogenesis. *RNA* **19**: 1064–1077.
- Vasileva A, Tiedau D, Firooznia A, Muller-Reichert T, Jessberger R. 2009. Tdrd6 is required for spermiogenesis, chromatoid body architecture, and regulation of miRNA expression. *Curr Biol* **19**: 630–639.
- Vourekas A, Zheng Q, Alexiou P, Maragkakakis M, Kirino Y, Gregory BD, Mourelatos Z. 2012. Mili and Miwi target RNA repertoire reveals piRNA biogenesis and function of Miwi in spermiogenesis. *Nat Struct Mol Biol* **19**: 773–781.
- Vourekas A, Zheng Q, Fu Q, Maragkakakis M, Alexiou P, Ma J, Pillai RS, Mourelatos Z, Wang PJ. 2015. The RNA helicase MOV10L1 binds piRNA precursors to initiate piRNA processing. *Genes Dev* **29**: 617–629.
- Watanabe T, Cheng EC, Zhong M, Lin H. 2015. Retrotransposons and pseudogenes regulate mRNAs and lncRNAs via the piRNA pathway in the germline. *Genome Res* **25**: 368–380.

- Xu M, You Y, Hunsicker P, Hori T, Small C, Griswold MD, Hecht NB. 2008. Mice deficient for a small cluster of Piwi-interacting RNAs implicate Piwi-interacting RNAs in transposon control. *Biol Reprod* **79**: 51–57.
- Zhang Z, Xu J, Koppetsch BS, Wang J, Tipping C, Ma S, Weng Z, Theurkauf WE, Zamore PD. 2011. Heterotypic piRNA Ping-Pong requires qin, a protein with both E3 ligase and Tudor domains. *Mol Cell* **44**: 572–584.
- Zhang Z, Koppetsch BS, Wang J, Tipping C, Weng Z, Theurkauf WE, Zamore PD. 2014. Antisense piRNA amplification, but not piRNA production or nuage assembly, requires the Tudor-domain protein Qin. *EMBO J* **33**: 536–539.
- Zhang P, Kang JY, Gou LT, Wang J, Xue Y, Skogerboe G, Dai P, Huang DW, Chen R, Fu XD, et al. 2015. MIWI and piRNA-mediated cleavage of messenger RNAs in mouse testes. *Cell Res* **25**: 193–207.



## RNF17 blocks promiscuous activity of PIWI proteins in mouse testes

Kaja A. Wasik, Oliver H. Tam, Simon R. Knott, et al.

*Genes Dev.* 2015, **29**: originally published online June 26, 2015  
Access the most recent version at doi:[10.1101/gad.265215.115](https://doi.org/10.1101/gad.265215.115)

---

### Supplemental Material

<http://genesdev.cshlp.org/content/suppl/2015/06/24/gad.265215.115.DC1>

### References

This article cites 60 articles, 23 of which can be accessed free at:  
<http://genesdev.cshlp.org/content/29/13/1403.full.html#ref-list-1>

### Creative Commons License

This article is distributed exclusively by Cold Spring Harbor Laboratory Press for the first six months after the full-issue publication date (see <http://genesdev.cshlp.org/site/misc/terms.xhtml>). After six months, it is available under a Creative Commons License (Attribution-NonCommercial 4.0 International), as described at <http://creativecommons.org/licenses/by-nc/4.0/>.

### Email Alerting Service

Receive free email alerts when new articles cite this article - sign up in the box at the top right corner of the article or [click here](#).

---



Biofluids too dilute to detect  
microRNAs? See what to do.

EXIQON